Paper

Conducted Emission Characteristics of an Active Snubber Boost Converter

Chaiya Tantisukarom* Non-member
Werachet Khanngern* Non-member
Shuichi Nitta** Life Member

In this paper, the conducted emission characteristics of an active snubber boost converter with proposed timing diagram are investigated and compared with its conventional boost converter. It is illustrated theoretically and experimentally that the soft switching technique can reduce the high switching dv/dt and di/dt rate, as well as the conducted emission noise spectra generated from the hard-switched counterpart effectively. The presented active snubber boost converter shows the line to ground and the neutral to ground conducted emission spectra significantly be improved at high frequency range over the hard-switched operation.

Keywords: Conducted Emission, Active Snubber, Boost Converter, Soft Switching

1. Introduction

The operation of the dc converter at high frequency has raised the electromagnetic noise interference (EMI) because of their switching action. For the noise, its propagation mode is either by the radiation or line conduction. The rate of changes of the voltage and current in power electronics converters are the main sources of the conducted emission [1][2]. There are two types of conducted emission noises produced on the main power supply. They are the differential mode (DM) and common mode (CM) noises. The DM noise propagates in and out of the converter circuit through its main input power line. While the CM noise flows in the same direction through its main input power lines with the stray capacitance coupled to the chassis ground reference plane. In this paper, the **line to ground** and the **neutral to ground** conducted emission characteristics of an active snubber boost converter are presented.

The boost converter is widely used in many applications because of its simple power and ground-reference control circuits. The conventional boost converter, which is known as a hard-switched operation, produces high dv/dt and di/dt rates. Those rates will cause a high switching loss and stress over the power switch. They are also perceived as the major sources of the conducted emission signals. Various active snubber (soft-switching) techniques for the boost converter have been proposed in the literature to reduce the switching loss and stress over the semiconductor power switches. They can evidently improve their power efficiencies. It also improves and extends the operating range [3]. The active snubber technique creates a zero voltage and/or zero current condition over the switch. The switch is then turned on or off softly. So, the instantaneous power losses occurring at the switching transition could effectively be reduced. The rate of changes of current and voltage are also reduced due to the soft-switched schemes. Because the conducted emission signals are proportional to the rate of change of voltage or current magnitudes, the low rate of change therefore reduces the conducted emission coupling effectiveness. The soft-switching technique is then conceivable in the reduction of the conducted EMI noise generated by the hard switching operation [1].

The active snubber boost converter presented in [3] is observed to be the experimental circuit for the conducted emission characteristics study. It is of interest from the excellent in a minimum number of components for the active snubber circuit. However, the voltage and current stresses of the components of the circuit in [3] are reported similar to the conventional hard-switched counterpart. The different control-timing diagram and its operating modes are proposed in this paper. With the new control diagram, the presented active snubber achieves the ZCS-ZVS condition. The conducted emission spectra; Line-to-Ground and Neutral-to-Ground, of the presented active snubber converter are then studied and compared with its conventional circuit.

The measured results show that the proposed soft switching technique can effectively mitigate the conducted emission over the high frequency range.

2. The Mechanism of the Conducted Emission Coupling

2.1 Inductive Coupling (Differential Mode: DM) The inductive coupling occurs from the close-loop of a current signal path. The power main DM noise

* Faculty of Engineering and Research Center for Communications and Information Technology, King Mongkut's Institute of Technology Ladkrabang (KMITL)
Bangkok, Thailand 10520. Phone/Fax: +662 737-3000 Ext. 3322
** Graduate School, Production System Engineering, Salesian Polytechnic
2-35-11, Igusa Suginami, Tokyo, 167-0021, Japan

current, I_{DM}, in an electrical circuit is illustrated in Fig. 1 [4].

In a close current loop of the single-phase two-wire system, the differential mode current flows in, from one of the power input line through the cable, wire, and interconnect represented by Z_{CIR}, to the load, Z_{LOAD}. It then flows out through the rest of the close interconnecting loop Z_{RTN} to the other end of the power return line. It will develop the differential mode voltage, V_{DM} as shown in Fig. 1.

The ac resistance of a copper wire [9] is given by Eq. (1),

$$R_{ac} = \left(0.244d\sqrt{f} + 0.26\right) \cdot R_{dc} \quad \cdots\cdots\cdots\cdots (1)$$

Where d is the diameter of the wire (cm), f is the frequency (Hz), and R_{dc} is the dc resistance (Ω). It can be seen from Eq. (1) that the ac resistance of a copper wire generally used as the interconnect varies with the frequency.

The inductance (or self-inductance) L is defined [7] in Eq. (2) as the ratio of the total flux Φ of the linear magnetic media linkages to the current I flowing in the N-turn coil which they link, or

$$L = \frac{N\Phi}{I} \quad \cdots\cdots\cdots\cdots\cdots\cdots\cdots\cdots\cdots\cdots (2)$$

The magnetic flux Φ is defined as in Eq. (3),

$$\Phi = \int_s B \cdot ds \quad \cdots\cdots\cdots\cdots\cdots\cdots\cdots\cdots\cdots\cdots (3)$$

Where $\boldsymbol{B}$ is the magnetic flux density and $\boldsymbol{ds}$ is any designated closed area. It is to be noted from Eq. (3) that the inductance, Eq. (2), depends on the physical structure.

The impedance of a wire with a circular cross section at least 15 cm from a ground structure is given [9] by Eq. (4).

$$L = 0.002l\left(2.303\log\left(\frac{4l}{d}\right) - 1 + \frac{\mu_r}{4}\right)(\mu\mathrm{H}) \cdots (4)$$

Where l is the length of the wire (cm), d is the diameter (cm), and μ_r is the relative permeability. The inductance calculation from other specific physical structures could be valuably found more in [5] [6].

The principle of the DM coupling is then defined fundamentally on the di/dt and the inductive reactance. The induced voltage across the inductor is given by

$$v_L = L \cdot \left(\frac{di}{dt}\right) \quad \cdots\cdots\cdots\cdots\cdots\cdots\cdots\cdots\cdots\cdots (5)$$

Where, L is a closed loop inductor.

The induced voltage v_L, produces the unwanted differential mode signals. To minimize it, from Eq. (5), the inductance L must be kept as low as possible. To achieve this, any interconnection that realizes a high di/dt rate must be kept as short as possible. In general, all interconnects, printed wiring board (PWB) track, wiring, and cabling are needed to keep as short as possible also.

The active snubber presented in this paper comes with the snubber inductor, L_{r}, (as shown in Fig. 4). It is used to limit the di/dt rate for the power-diode at turn-off and the auxiliary-switch at turn-on states. The latter case generates the zero current switch (ZCS) turn-on condition for the auxiliary switch. From Eq. (5), the reduction of the circuit di/dt in the presence of the snubber inductor L_{r}, reduces the induced voltage v_L. It mitigates the conducted emission.

2.2 Capacitive Coupling (Common Mode: CM) The capacitance of a portion of the infinite-plane arrangement [7] having a surface area S whose linear dimensions is much greater than the separation d, is shown in Eq. (6),

$$C = \frac{\varepsilon S}{d} \quad \cdots\cdots\cdots\cdots\cdots\cdots\cdots\cdots\cdots\cdots (6)$$

Where C is the designed capacitor, ε is the permittivity of the dielectric between two plates (F/m) and d is the distance between the plates (m). The common mode noise is recognized in the presence of the earth system [10]. Let consider the node $\mathrm{L_g}$ and $\mathrm{N_g}$ referred to the chassis ground shown in Fig. 2, they may form the capacitors C_{CM1} and C_{CM2}, respectively.

The fundamental equation of the current, which flows into the capacitor, is

$$i_C = C \cdot \left(\frac{dv}{dt}\right) \quad \cdots\cdots\cdots\cdots\cdots\cdots\cdots\cdots\cdots\cdots (7)$$

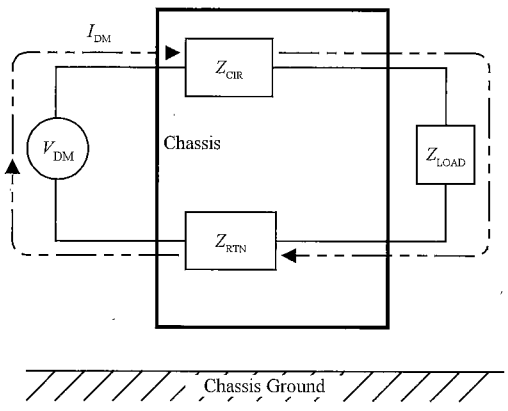

Fig. 1. Differential mode (DM) current path.

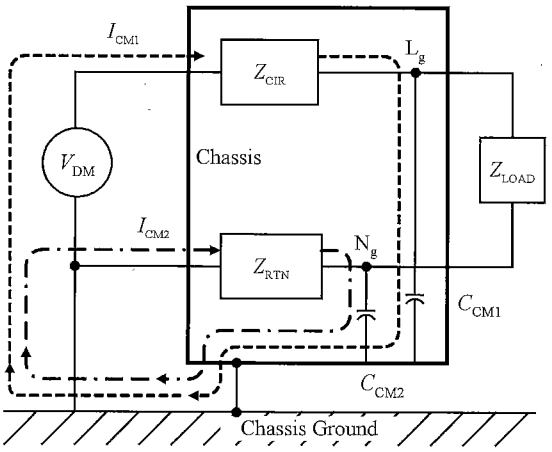

Fig. 2. Commode mode current path.

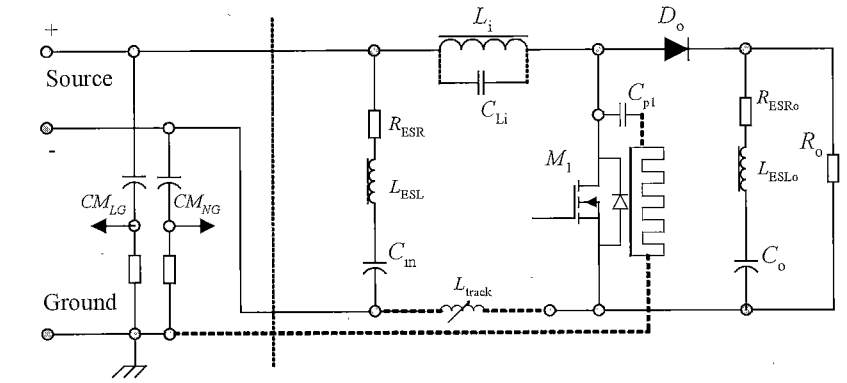

(a) Conventional boost converter.

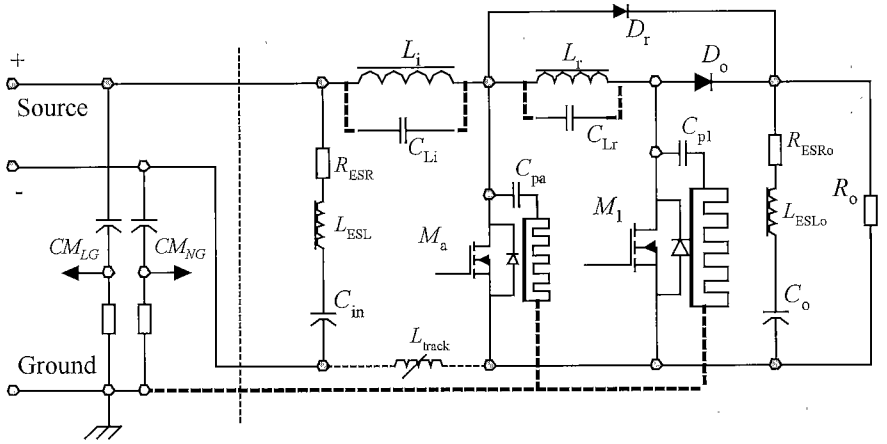

(b) Experimental active snubber boost converter.

Fig. 3. Simplified boost converter including parasitic elements: (a) conventional boost converter and (b) experimental active snubber boost converter.

From Eq. (6), a piece of surface respecting to the chassis ground may form a capacitor. It then may couple a current from the dv/dt rate represented by Eq. (7), to the chassis ground. This capacitor is usually called a *stray* or *parasitic* capacitor. When the connection between the circuit and chassis ground is implemented, the common mode current, I_{CM1} and I_{CM2}, are taken in place as shown in Fig. 2 [4].

To minimize the capacitive coupling effectiveness, it is to keep the area of those plates forming a parasitic capacitor as small as possible and/or increase the distance d. Since the heat sink should be grounded, the relative permittivity ε_r of the electrical isolator placed between the switching component package and the heat sink must be carefully selected to minimize the parasitic capacitance.

The active snubber circuit in this paper is designed to control the rate of change of voltage at the switching transient. The Zero Voltage Switch (ZVS) condition is to bring down the voltage across the targeted power switch to be nearly zero before it is turned on. Under the ZVS interval, the turn-on switching loss is minimized. The instantaneous power loss generated at the turn on switching transition could be obviously reduced. The stress over the switch is also reduced to the minimum. It leads to the reduction of the required size of the heat sink.

Fig .3 illustrates the parasitic elements such as C_{Li}, C_{p1} as shown in dotted lines for the conventional in Fig. 3(a). The parasitic elements of the presented active snubber boost converter is depicted in Fig. 3(b). These parasitic elements characterize the conducted emission coupling mechanism. The parasitic element L_{track}, on the return path in Fig. 3, represents a total interconnecting inductive reactance. The practical inductor also has the stray capacitor, C_{Lx}, from its physical structure [11]. The common mode parasitic capacitor, C_{p1} & C_{pa}, which is formed between the high dv/dt node and the grounded heat sink, will couple the noise current to the chassis ground. All of the parasitic elements depend on the frequency.

In conclusion, any changing in the physical aspect such as a wiring, an interconnect, or a device placement, and the electrical aspect such as a difference in a semiconductor power rating, type, or packaging, and the soft-switched topology itself will directly effect the conducted emission coupling performance.

The contributions of the differential mode, I_{DM}, and the common mode, I_{CMx}, current components to the measured conducted emission spectra revisited in this section is depicted in the section 4, Fig. 8(b).

3. Experimental Circuit and Operating Conditions

To carry out the study of the conducted emission characteristics of an active snubber boost converter, the 200-

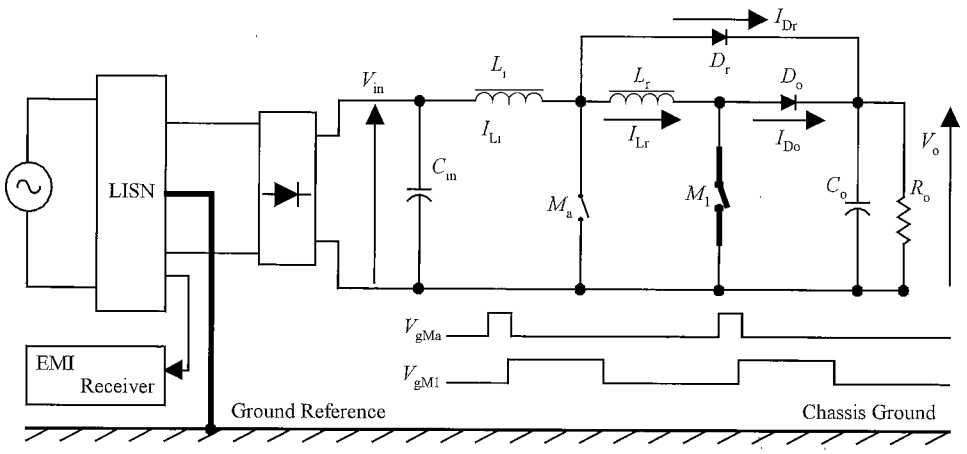

Fig. 4. Active snubber boost converter for experiment.

watt single-phase dc boost converter, in Fig. 4, with proposed control timing diagram, Fig. 5(g), is constructed.

The ratings of the experimental circuit in Fig. 4 are as follows:

V_{in}: 100 V, C_{in}: 22,000 μF, L_i: 470 μH, L_r: 10 μH, C_o: 470 μF, M_a: IRF840, M_1: IRFP460, D_o and D_r: MUR860, Switching frequency: 100 kHz, and 200-watt output.

The analysis of the proposed control-timing diagram of the ZCS-ZVS active snubber boost converter shown in Fig.5 is derived. The operation modes and the ideal key waveforms are shown in Fig. 5(a)–(g). The auxiliary switch M_a is turned on before turning on the main switch M_1. To simplify the analysis, the boost converter will be assumed to be an ideal circuit and operated in the continuous conduction current mode. However the output capacitance (C_{oss}) and the body diode of the MOSFET switch, which are not shown in Fig. 5, will be included into the operation analysis. As shown in Fig. 5, four operation modes are included in one switching cycle.

Before 0, the current from the boost inductor I_{Li} flows to the load through the snubber inductor L_r and the boost power diode D_o. The two power-switches M_a and M_1, and the snubber diode D_r are in the off state.

Mode-1: *Interval* 0-1. The gate signal of the auxiliary switch M_a is applied to turn on the switch M_a. Since the current I_{Li} is hanged up with the boost inductor and the snubber inductor, the current between these inductors could not be changed immediately. The current in the auxiliary switch will ramp up from zero to the maximum value with the slope of

$$\frac{di_{Ma}}{dt} = \frac{V_o}{L_r} \quad \cdots\cdots (8)$$

The current in the boost power diode I_{Do} and the current in the snubber inductor I_{Lr} will decrease at the same rate as in Eq. (8). The boost power diode D_o will then stop conducting softly. At this moment, the output capacitance of the MOSFET switch M_1 (Fig. 4, not shown) starts discharging through the snubber inductor L_r. When the capacitance is fully discharged, the voltage across the switch becomes zero. The current I_{Lr} will flow through the body diode (not shown) of the switch M_1. The gate signal of the main switch is applied at this point of time to achieve the turn-on ZVS condition.

For the practical circuit, the gate signal of M_1 should be applied before taking off the gate signal of M_a (condition #1 in Fig. 5) to guarantee the ZVS condition.

The critical delay time before applying the gate signal of M_1 (condition #2 in Fig. 5) is to wait until the boost power diode, D_o, completely turns off.

Mode-2: *Interval* 1-2. Entering this mode, the main switch M_1 is already turned on. When the auxiliary switch is turned off, the current from the boost inductor I_{Li} is 'kicked' out to the load through the active snubber D_r. Since the active snubber diode is conducted, the output voltage is appeared over the auxiliary switch in this mode.

The snubber diode current I_{Dr} then decreases under the influence of the snubber inductor L_r since the main current is conducting by the main switch M_1. It will stop conducting softly.

Mode-3: *Interval* 2-3. The auxiliary switch M_a is in the off state. The main switch M_1 is turned on. It is an equivalent to the energy boost stage in the boost inductor L_i as similar to the conventional boost circuit.

Mode-4: *Interval* 3-4. This mode is also considered as equivalence to the free wheeling stage of the conventional boost converter. At the end of this mode, it is to be noted that the main switch M_1 is turned off under the same stress as in hard-switched circuit.

Fig. 6 shows the measured waveforms of the gate control signals Vg_{Ma}, Vg_{M1}, and the currents of the boost inductor I_{Li} and the snubber inductor I_{Lr}, respectively. It is in a good trend with the analysis proposed waveforms in Fig. 5.

In Fig. 7 the measured waveforms of the power diode current I_{Do}, and the snubber diode current I_{Dr} are shown with the inductor current waveforms I_{Li} and I_{Lr}, respectively. They are also in a good trend with the analysis ones.

The experimental converter is comprised of 3 PCBs, which are the power, the driver, and the base-frequency units. They are incorporated on the open chassis ground plate. The proposed control-timing diagram improves

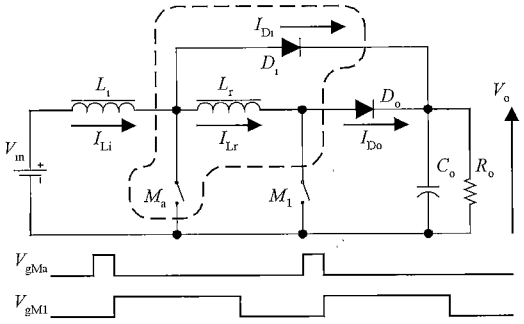

(a) The presented Circuit.

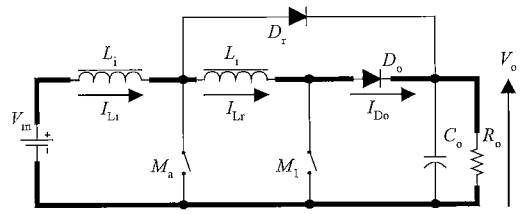

(b) Before 0.

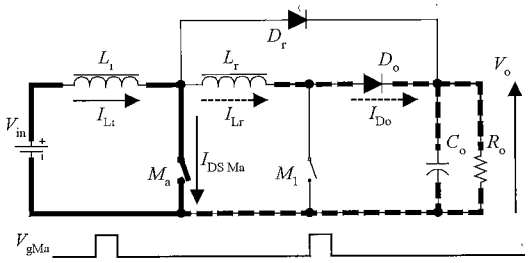

(c) Mode-1.

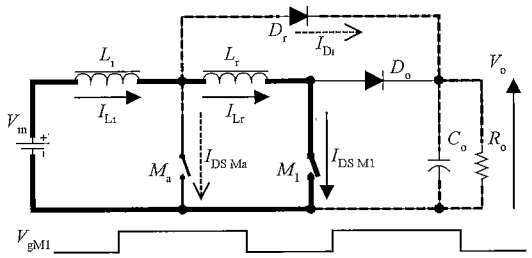

(d) Mode-2.

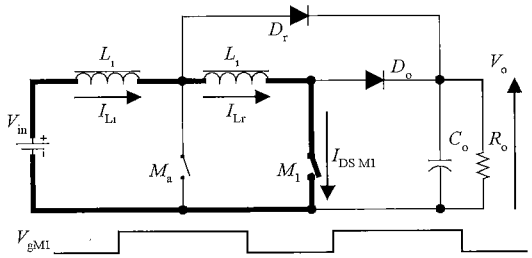

(e) Mode-3.

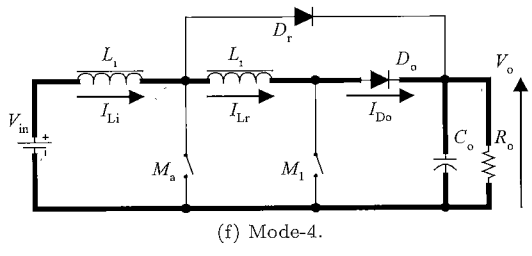

(f) Mode-4.

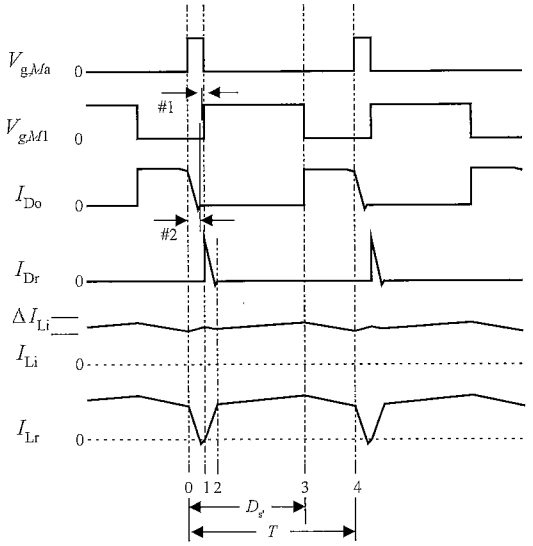

(g) Proposed control diagram.

Fig. 5. Operation modes and the analysis of the ideal key waveforms.

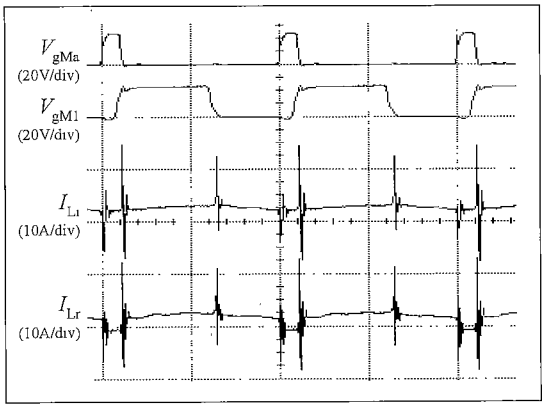

Fig. 6. Measured waveforms of gates and inductors currents, [x-axis: 5 μs/div].

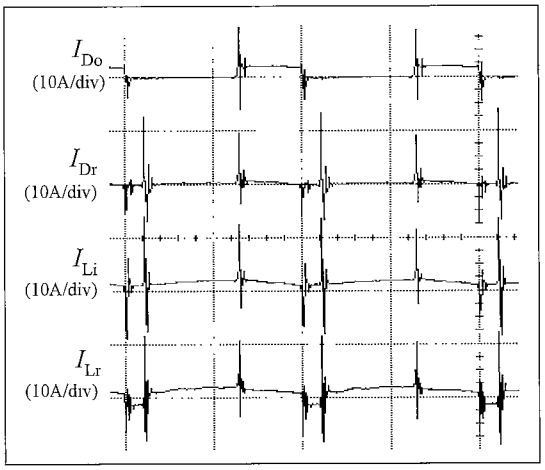

Fig. 7. Examples of key current waveforms, [x-axis: 5 μs/div].

the low line power efficiency by 4%. The proposed control-timing diagram provides the power efficiency better than 92% compared to 88% of the experimental converter without the active snubber circuit at the

same rated power.

With the proper algebraic analysis using that the *average voltage* across an inductor over one switching period is equal to zero, the voltage gain of the experimented active snubber boost converter, Appendix A, is shown in Eq. (9),

$$V_o = V_{in}\frac{1}{(1-D_{s'})}\frac{1}{\left(1+\dfrac{L_r}{D_{s'}R_o t_{off'}}\right)} \cdots\cdots (9)$$

The ripple current in the boost inductor [2] is then expressed by Eq. (10),

$$\Delta I_{L_i} = \frac{V_o T}{L_i}\left(D_{s'}(1-D_{s'}) + \frac{L_r}{R_o}\right) \cdots\cdots (10)$$

The frequency characteristic of the ripple current, $f_r(t)$, can be obtained by using the Fourier series analysis, Appendix B, as shown in Eq. (11),

$$f_r(t) = A_0 + \sum_{n=1}^{\infty} A_n \cos\left(\frac{n\pi t}{T} + \phi_n\right) \cdots\cdots (11)$$

Where $A_0 = \Delta I_{L_i}$, $A_n = 2|C_n|$, $\phi_n = \arg C_n$, and Eq. (12) is obtained.

$$C_n = \frac{\Delta I_{Li}}{Ta}\left[Te^{aT} - \frac{e^{aT}}{a} + D_{S'}e^{a\left(1-\frac{t_{off'}}{T}\right)} - \frac{e^{a\left(1-\frac{t_{off'}}{T}\right)}}{a} - \frac{1}{a}\right] \cdots\cdots (12)$$

where, $a = -j2n\frac{\pi}{T}$, T = Effective switching period, $D_{s'}$ = Effective turn on duty ratio, and $t_{off'} = (1-D_{s'})\cdot T$.

From Eq. (9), the snubber inductor L_r effects directly to the ripple current. It also effects to the frequency characteristic of the ripple current (ΔI_{L_i}) shown in Eq. (10), (11), and (12).

4. Test Set Up for the Comparison between the Proposed Active Snubber and its Conventional Boost Converter

The presented active snubber boost converter is measured at first. Then, the 'active snubber set' is taken out for the second measurement represented the conventional boost converter. The layout of the tested circuit is the same for both measurements. The snubber inductor L_r is replaced by the same size of wire. The snubber diode D_r, and the auxiliary switch M_a are taken out. However, the switch M_a and its heat sink are placed and grounded at the same location as in the first measurement.

4.1 Circuit Model of the Conducted Emission Measurement The Line Impedance Stabilization Network (LISN) as shown in Fig. 8(a) is used to provide firstly the specified impedance over the working radio frequencies range at the terminals of the unit under test. It has to provide sufficient isolation the test circuit from spurious or unwanted interference signals on the supply mains [8]. It is used to couple the measuring disturbance voltage to the EMI receiver. It also has

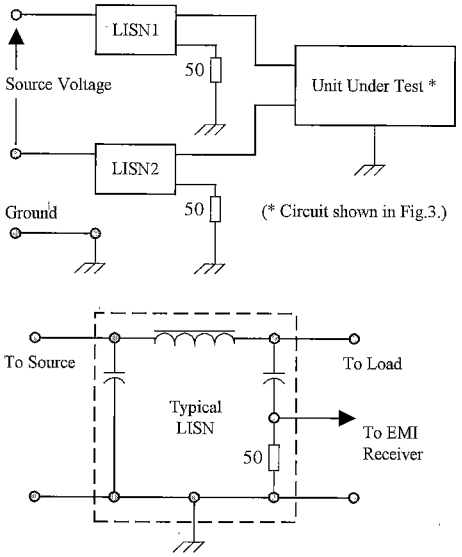

(a) Typical Line Impedance Stabilization Network (LISN) arrangement for the conducted emission measurement.

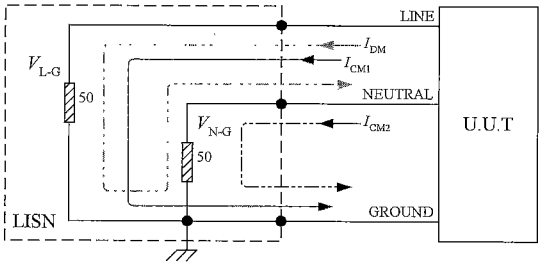

(b) The contributions of the differential mode and the common mode current components on the measured conducted emissions.

Fig. 8. The conducted emission measurement.

to prevent the main voltage from being applied to the measuring receiver.

The impedance of a LISN is the magnitude of the impedance with respect to the reference earth measured at an equipment terminal when the corresponding disturbance output terminal is terminated with 50 Ω.

Fig. 8(b) illustrates the contributions of the differential mode, I_{DM}, and the common mode, I_{CMx}, current components described in the section 2, on the measured conducted emission signals over the completed LISN arrangement [12]. From Fig. 8(b), the differential mode current flows down through one 50 Ω resistor and up through the other one. The common mode currents flow down though both 50 Ω resistors. The contributions due to each current add in the $V_{L\text{-}G}$ and subtract in the $V_{N\text{-}G}$. If the DM and the CM currents are of the same magnitude, the Line to Ground and the Neutral to Ground spectra will not be the same.

The Agilent E7401A EMC Analyzer is used as the emission receiver and display. The experimental unit under test chassis ground is connected to the RF ground point of the EMCO 3810/2 LISN. The Receiver and the LISN are grounded to the building earth. The load is the 2 pieces of 100 watts incandescent lamps. The *peak-hold* mode of the EMI receiver is selected to measure the 0.15–30 MHz conducted emission spectrum. This model of LISN is able to measure the line to ground and the

neutral to ground conducted emission using a selector switch.

The measurement is then carried out, in the EMC Labs of the King Mongkut's institute of Technology Ladkrabang, without enclosure and filter. This paper presents the Line to Ground and the Neutral to Ground conducted emission characteristics measured from the experimental circuit in section 3.

5. The Conducted Emission Characteristics Investigation

The measured waveforms of the current and voltage of the main, M_1, and the auxiliary, M_a, switches of the experimented active snubber boost converter are shown in Fig.9. The soft switching conditions over the switches are depicted in Fig. 9. The ZCS condition is achieved over the auxiliary switch, M_a, at turn on while the main switch, M_1, is turned on at the ZVS condition.

It could be noted that the high dv/dt at turn on state takes place in the operation over the auxiliary switch, M_a, as shown by the waveform$V_{DS\ Ma}$ in Fig. 9. The auxiliary switch M_a, achieves the ZCS condition at turn on. The switch is modeled comprised of the R-L-C element for the high frequency as the lumped ideal component (LIC) switch [13]. The noise developed over the L element of the switch is limited, (di/dt is limited) under the ZCS condition. The voltage change developed over the stray capacitor should be considered less than the unlimited di/dt. Its noise coupling effectiveness to ground under ZCS condition is considered lower than the one in the hard switching mode.

When the auxiliary switch M_a is turned off, the current from the boost inductor, L_i, is kicked to the load through the snubber diode, D_r. The output voltage is realized (circled in Fig. 9—Operation Mode-2), over the switch M_a until the auxiliary diode D_r stops conducting. This voltage stress over the auxiliary switch is considered to exceed that one in the conventional boost converter.

From the voltage, $V_{DS\ M1}$, and the current $I_{DS\ M1}$ waveforms of the main switch M_1, in Fig. 9, they show the ZVS condition at turn on achievement of the proposed control-timing diagram. It is seen at the ZVS condition in Fig. 9 that the turn on voltage transient of the main switch is significantly reduced nearly to be zero. At the free wheeling interval, the experimented active snubber boost converter is considered to be identical to the conventional boost converter.

The voltage transient conditions investigated above may be concluded that the conducted emission performance at a low frequency range compared the proposed active snubber with its conventional counterpart will mostly show the same result. Because the *effective* desired *waveforms* are considered to be similar between the two converters, except only the transients. The voltage transient stresses on switching devices are limited by the proposed soft-switched operation. It could be concluded that the proposed soft switching technique could mitigate the conducted emission more effectively over the high frequency range. The result of the investigation will be examined experimentally.

6. Measurement Results

Measured spectra are shown in Fig. 10 and 11 for the

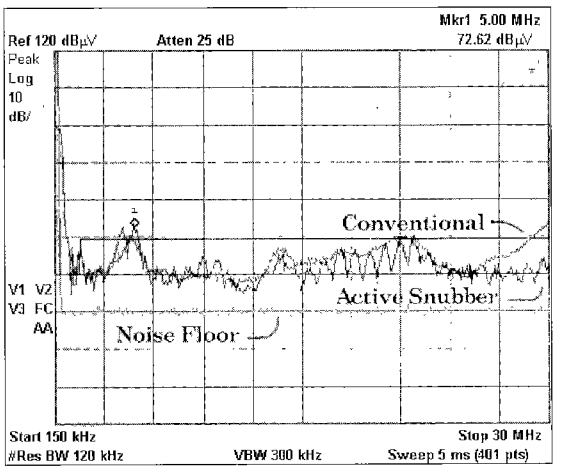

Fig. 10. Conducted emission spectrum of Line to Ground.

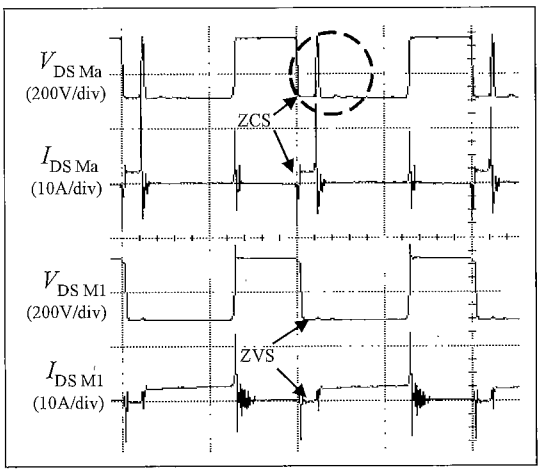

Fig. 9. Zero Current M_a, and Zero Voltage M_1, Switches, [x-axis: 5 μs/div].

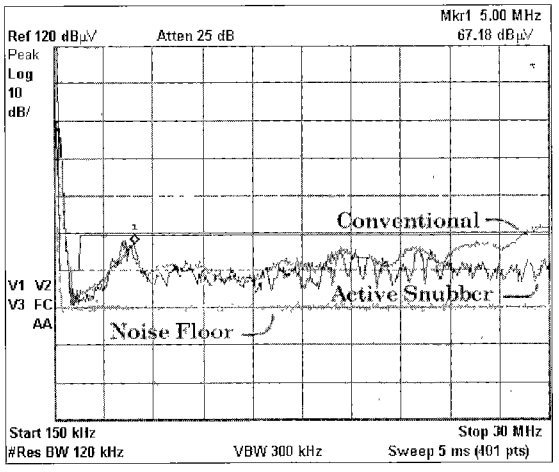

Fig. 11. Conducted emission spectrum of Neutral to Ground.

conducted emission from the Line-to-Ground and the Neutral-to-Ground, respectively. In those Figures, the spectra are compared the active snubber with the conventional boost converters. As investigated in section 5, the measured results show similar spectra at the low frequency bandwidth. Under a certain circumstance, the active snubber noise performance may be worse than the conventional boost converter. This is due to more circuit components sensitive to the conducted emission coupling are included. They could form other self-resonance frequencies over the original circuit components.

Since the main switch M_1 has much reduced in the dv/dt rate, the measured spectra of the proposed active snubber converter show better result than its conventional boost converter at the high frequency range.

The measurement is carried out in the open area of the KMITL EMC Labs test-table. The uncertainty of the measurement is necessitated to take into account when the regulation pre-compliance is in consideration. The FCC15 AC limit line is loaded into both figures for the reference purpose only. The noise floor is measured when the main power supply is turned off.

7. Conclusion

The conducted emission characteristics of a ZCS-ZVS active snubber boost converter are presented and investigated experimentally. Its coupling mechanism fundamentals are described. The measured results show that the proposed soft switching technique can effectively mitigate the conducted emission over the high frequency range.

The degree of the conducted emission mitigation directly depends on the converter topology, the detail of the applied soft-switching technique, the physical wiring and layout, the semiconductor switch device itself, the proper circuit design, and all of the electromagnetic related elements. It could be notified that the solution developed successfully for a circuit might not be *fully* applied to the other ones. For the interested circuit, it has to be investigated by its own topology and design.

The fundamental of the conducted electromagnetic coupling mechanism, which substantially presented in this paper, can generally be applied to the conducted noise reduction knowledge of the high switching frequency power electronics circuits.

(Manuscript received March 22, 2002,
revised Oct. 28, 2002)

References

(1) Y. Tang, H. Zhu, B. Song, J.S. Lai, and C. Chen: "EMI Experimental Comparison of PWM Inverters Between Hard- and Soft-Switching Techniques", *IEEE Power Electronics in Transportation*, pp.71–77 (1998-10)

(2) Q. Chen: "Electromagnetic Interference (EMI) Design Considerations for a High Power AC/DC Converter", *Power Electronics Specialists Conference*, 1998. PESC 98 Record. 29th Annual IEEE, Vol.2, 17-22, pp.1159–1164 (1998-5)

(3) M.M. Jovanovic and Y. Jang: "A Novel Active Snubber for High-Power Boost Converters", *IEEE Trans. on Power Electronics*, Vol.15, No.2, pp.278–284 (2000-3)

(4) J.C. Fluke: "Controlling Conducted Emission By Design", Van Nostrand Reinhold (1991)

(5) F.B.J. Leferink: "Inductance Calculations; Methods And Equations", *International Symposium on Electromagnetic Compatibility* 1995, 14-18, pp.16–22 (1995-8)

(6) F.B.J. Leferink: "Inductance Calculations; Experimental Investigations", *International Symposium on Electromagnetic Compatibility* 1996, 19-23, pp.235–240 (1996-8)

(7) W.H. Hayt, Jr.: Engineering Electromagnetics, McGraw-Hill., 1981., 4th Edition, pp.127–169 (1981)

(8) T. Williams: EMC for Product Designers, B-H NEWNES, 1992. 2nd Edition, p.70 (1992)

(9) D.A. Weston: Electromagnetic Compatibility: Principles and Applications, Marcel Dekker, Inc. 1991., pp.206–214 (1991)

(10) K. Armstrong: "Earth? What Earth?", *Shielding and Grounding (Ref. No. 2000/016), IEE Seminar on*, 27 Jan., pp.2/1–2/8 (2000)

(11) A. Massarini, M.K. Kazimierczuk, and G. Grandi: "Lumped Parameter Models for Single- and Multiple-Layer Inductors", *PESC '96 Record, 27th Annual IEEE*, 23-27 June 1996, vol.1, pp.295–301 (1996)

(12) C.R. Paul: Introduction to Electromagnetic Compatibility, John Wiley & Son, Inc., pp.450–455 (1992)

(13) C. Tantisukarom, V. Tarateeraseth, W. Khan-ngern, and S. Nitta: "The Lump-Ideal-Component (LIC) Switch Micro Signal Concept for the Conducted Emission Analysis", *PESC'02 Record, 33th Annual IEEE*, 23-27 June (2002)

Appendix

Appendix A

Voltage gain of the proposed active snubber boost converter circuit.

The average voltage in one switching cycle is zero, then from app. Fig. 1,

$$V_1 t_{01} + (V_1 - V_o)\, t_{12} + (V_1 - V_{Lr})\, t_{23} + (V_1 - V_{Lr} - V_o) t_{34} = 0 \quad \cdots\cdots\cdots\cdots \quad \text{(A1)}$$

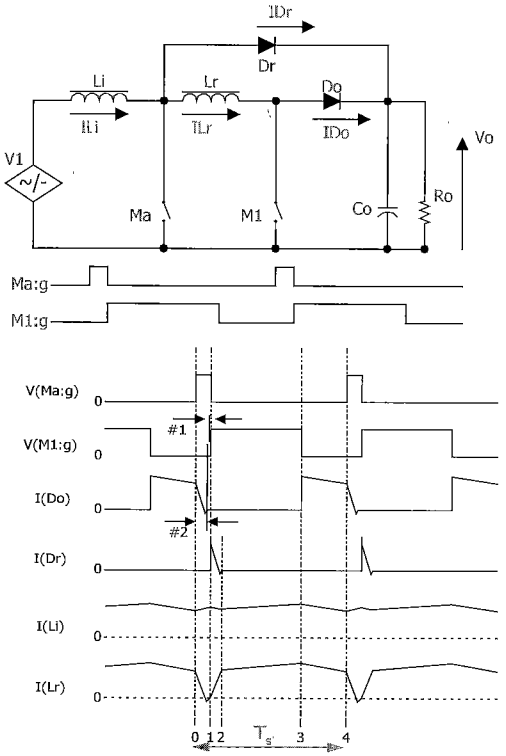

app. Fig. 1. The circuit and the timing diagram used to derive the voltage gain.

$$V_1 t_{01} + V_1 t_{12} - V_o t_{12} - V_o t_{12} + V_1 t_{23} - V_{Lr} t_{23} + V_1 t_{34} - V_{Lr} t_{34} - V_o t_{34} = 0 \cdots\cdots (A2)$$

$$V_1 (t_{01} + t_{12} + t_{23} + t_{34}) - V_{Lr} (t_{23} + t_{34}) - V_o (t_{12} + t_{34}) = 0 \cdots\cdots (A3)$$

$$V_o (t_{12} + t_{34}) = V_1 (t_{01} + t_{12} + t_{23} + t_{34}) - V_{Lr} (t_{23} + t_{34}) \cdots\cdots (A4)$$

At steady state, the average voltage across Lr in one switching cycle is zero. Then V_{Lr}=0, Eq. (A4) will be as follows

$$V_o = V_1 \frac{t_{s'}}{(t_{12} + t_{off'})} \cdots\cdots (A5)$$

$$t_{s'} = (t_{01} + t_{12} + t_{23} + t_{34}), \text{ and } t_{off'} = t_{34} \cdots\cdots (A6)$$

Assume $D_{s'} = \frac{t_{s'} - t_{34}}{t_{s'}}$, then $D_{s'} = 1 - \frac{t_{off'}}{t_{s'}}$, and $t_{s'} = \frac{t_{off'}}{1 - D_{s'}}$, replaced in Eq. (A5) gets

$$V_o = V_1 \frac{1}{(1 - D_{s'})} \frac{t_{off'}}{(t_{12} + t_{off'})} \cdots\cdots (A7)$$

$$V_o = V_1 \frac{1}{(1 - D_{s'})} \frac{1}{\left(\frac{t_{12}}{t_{off'}} + 1\right)} \cdots\cdots (A8)$$

To find out the value of t_{12}

$$V_{L_r} = L_r \frac{di_{L_i}}{dt}, \quad \Delta t_{12} = \frac{L_r}{V_{L_r}} \Delta I_{L_i}, \quad I_{R_o} = I_{L_i} D_{s'},$$

$$\Delta I_{L_i} = \frac{\Delta I_{R_o}}{D_{s'}} \cdots\cdots (A9)$$

$$\Delta t_{12} = \frac{L_r}{V_{L_r}} \frac{\Delta I_{R_o}}{D_{s'}} \cdots\cdots (A10)$$

Replace $V_{L_r} = V_o$ and $\Delta I_{R_o} = \frac{V_o}{R_o} = I_{R_o}$ in Eq. (A10)

$$\Delta t_{12} = \frac{L_r}{V_o} \frac{1}{D_{s'}} \frac{V_o}{R_o}, \quad t_{12} = \frac{L_r}{D_{s'} R_o} \cdots\cdots (A11)$$

Then replace t_{12} into Eq. (A8) yields

$$V_o = V_1 \frac{1}{(1 - D_{s'})} \frac{1}{\left(1 + \frac{L_r}{D_{s'} R_o t_{off'}}\right)} \cdots\cdots (A12)$$

The current ripple of the input inductor for the conventional boost circuit is

$$\Delta I_L = \frac{V_{in}}{L} D T_s \cdots\cdots (A13)$$

Assume that the current ripple caused by I_{Lr} is negligible compared to I_{L1}, replace Vo from Eq. (A12) into Eq. (A13) gets the current ripple of the proposed circuit

$$\Delta I_{L_1} = \frac{V_o T_s}{L_1} \left(D_{s'} (1 - D_{s'}) + \frac{L_r}{R_o}\right) \cdots\cdots (A14)$$

Appendix B

The frequency characteristic of the ripple current, $f_r(t)$

In order to maintain the equality of the phases at the positive frequencies between the complex and real representations, a cosinusoidal expansion

$$f(t) = A_0 + \sum_{n=1}^{\infty} A_n \cos\left(\frac{2n\pi t}{T} + \phi_n\right) \cdots\cdots (A15)$$

of the real Fourier series is the frequency adopted as an alternative to the sinusoidal series expansion.

The phase angle is defined as

$$\sin(\phi_n) = -\frac{b_n}{A_n} \text{ or } \cos(\phi_n) = -\frac{a_n}{A_n} \cdots\cdots (A16)$$

where $A_n = \sqrt{(a_n^2 + b_n^2)}$

$$f_r(t) = k_1 t_{01} - k_2 t_{12} + k_3 t_{23} - k_4 t_{34} \cdots\cdots (A17)$$

Where $0 < t_{01} \leq t_1$, $t_1 < t_{12} \leq t_2$, $t_2 < t_{23} \leq t_3$, and $t_3 < t_{34} \leq t_4$.

$k_1 = \frac{V_{in}}{L_i}$, $k_2 = \frac{V_o - V_{in}}{L_i}$, $k_3 = \frac{V_{in} - V_{Lr}}{L_i + L_r}$, and $k_4 = \frac{V_o - V_{Lr} - V_{in}}{L_i + L_r}$, (using the variable from Fig. 5 in the paper).

At steady state, it could be assumed that, $V_{L_r} \ll V_{L_i}$, and $L_r \ll L_i$, Then

$$f_r(t) = A_0 + \sum_{n=1}^{\infty} A_n \cos\left(\frac{2n\pi t}{T} + \phi_n\right) \cdots\cdots (A18)$$

Where $A_0 = \Delta I_{L_i}$, $A_n = 2|C_n|$, $\phi_n = \arg C_n$ and $C_n = \frac{1}{T} \int_0^T f_r(t) e^{\frac{-j2n\pi t}{T}} dt$

The boundary of the first point to enter the ZVS condition is subject to a load current. It is assumed that $t_{01} = t_{12}$ for the simplicity of the analysis as shown in app. Fig. 2.

The solution of the C_n is then

$$C_n = \frac{1}{T} \left(\int_0^{t_1} f_r(t) e^{\frac{-j2n\pi t}{T}} dt + \int_{t_1}^{t_2} f_r(t) e^{\frac{-j2n\pi t}{T}} dt + \int_{t_2}^{t_3} f_r(t) e^{\frac{-j2n\pi t}{T}} dt + \int_{t_3}^{t_4} f_r(t) e^{\frac{-j2n\pi t}{T}} dt \right) \cdots\cdots (A19)$$

To solve for C_n, let $t_{01} = t_{12} = D_a$, $k_3 = k_1$, $k_4 = k_2$, then

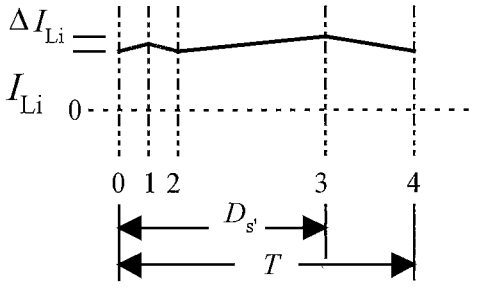

app. Fig. 2. The boundary first point to enter the ZVS condition boost inductor current waveform, $t_{01} = t_{12}$.

$$C_n = \frac{1}{T}\left(\int_0^{D_a} f_r(t)e^{\frac{-j2n\pi t}{T}}dt + \int_{D_a}^{2D_a} f_r(t)e^{\frac{-j2n\pi t}{T}}dt + \int_{2D_a}^{D_{S'}} f_r(t)e^{\frac{-j2n\pi t}{T}}dt + \int_{D_{S'}}^{T_{S'}} f_r(t)e^{\frac{-j2n\pi t}{T}}dt\right) \cdots\cdots\cdots\cdots \text{(A20)}$$

Using $\int e^x dx = e^x$, $\int e^{ax}dx = \frac{e^{ax}}{a}$, and $\int xe^{ax}dx = \frac{e^{ax}}{a}\left(x - \frac{1}{a}\right)$, and let $a = -\frac{j2n\pi}{T_{S'}}$, the solution of the C_n is

$$C_n = \frac{1}{T}\left[k_1\left\{\frac{e^{at}}{a}\left(t-\frac{1}{a}\right)\right\}_0^{D_a} - k_2\left\{\frac{e^{at}}{a}\left(t-\frac{1}{a}\right)\right\}_{D_a}^{2D_a} + k_1\left\{\frac{e^{at}}{a}\left(t-\frac{1}{a}\right)\right\}_{2D_a}^{D_{S'}} - k_2\left\{\frac{e^{at}}{a}\left(t-\frac{1}{a}\right)\right\}_{D_a}^{2D_a}\right] \cdots\cdots\cdots \text{(A21)}$$

From app. Fig.2, using the average ripple current over a switching period, the coefficient is approximated as

$$C_n = \frac{k}{T}\left[\frac{T_{s'}}{a}e^{aT_{S'}} - \frac{e^{aT_{S'}}}{a^2} + \frac{D_{S'}}{a}e^{aD_{S'}} - \frac{e^{aD_{S'}}}{a^2} - \frac{1}{a^2}\right] \cdots\cdots\cdots\cdots\cdots\cdots\cdots\cdots \text{(A22)}$$

Let $t_{off'} = (1 - D_{S'})T_{s'}$, $T = T_{S'}$, $k = \Delta I_{L_i}$, and rearrange Eq. A22 gets

$$C_n = \frac{\Delta I_{L_i}}{Ta}\left[Te^{aT} - \frac{e^{aT}}{a} + \left(1 - \frac{t_{off'}}{T}\right)e^{a\left(1-\frac{t_{off'}}{T}\right)} - \frac{e^{a\left(1-\frac{t_{off'}}{T}\right)}}{a} - \frac{1}{a}\right] \cdots\cdots\cdots\cdots\cdots \text{(A23)}$$

And

$$\Delta I_{L_i} = \frac{V_o T}{L_i}\left(D_{s'}(1 - D_{s'}) + \frac{L_r}{R_o}\right) \cdots\cdots\cdots \text{(A24)}$$

Chaiya Tantisukarom (Non-member) was born in Cha-Am, Phetburi, Thailand, in 1962. He received the Master degree in electrical engineering with the outstanding level of the master thesis in 1988 from King's Mongkut's Institute of Technology Ladkrabang (KMITL). He was a lecturer at the faculty of engineering, KMITL in 1985 to 1988. He is currently working towards the Doctor degree of electrical engineering at KMITL. He is a member of the EMC Labs, Research Center of Communication and Information Technology (ReCCIT) under the cooperation from Japan International Cooperation Agency (JICA). His research activities include power electronics, soft-switched DC-DC converters, conducted emission, simulation modeling, and microcontroller design and development.

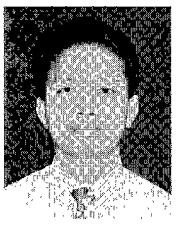

Werachet Khan-ngern (Non-member) was born in Ubonrachathani, Thailand, in 1960. He received B.Eng. and M.Eng. from King's Mongkut's Institute of Technology Ladkrabang (KMITL). He received the Ph.D. degree from Imperial College, University of London in 1997. His research areas are related in power electronics and electromagnetic compatibility (EMC). He is the EMC committee for Thai Industrial Standard Institute. He is also a member of working group of TC77B. Dr. W. Khan-ngern is currently an Assistant Professor at KMITL. He serves the KMITL as the EMC laboratory leader and the Vice Dean for the Academic Affairs of KMITL's Graduate School.

Shuichi Nitta (Life Member) earned BSEE and Ph.D. from Kyoto University and the University of Tokyo, 1960 and 1978, respectively. After working for an electric industry as a systems engineer and a quality assurance manager in computer area, he had been a professor of Tokyo University of Agriculture & Technology (TUAT) from 1985 to 2001. He retired the above university at the end of March in 2001 and become a professor emeritus of TUAT. Since April in 2001, he is currently a professor of Salesian Polytechnic. His research interests are EMC and Systems Maintainability and Safety. He is a member of IEEE, IEICE, SICEJ, Reliability Engineers Association of Japan, Society of Project Management and Association of Field Service Management International.